OCCURRENCE OF FELDSPATHIC ROCKS IN THE MARTIAN SOUTHERN HIGHLANDS. A. M. Sessa[1] and J. J. Wray[1], [1]Georgia Institute of Technology, Atlanta, GA (asessa3@gatech.edu).

Introduction: Currently, it is widely believed that the primary crustal material is basaltic in composition suggesting that magmatic differentiation (i.e., the production of late-stage melts from alkali-rich mantle sources) was not a key contributor to the production of the Martian crust [12]. However, various remote sensing, and recent in situ, studies utilizing instruments aboard MGS/Mars Odyssey (e.g., TES and THEMIS [3, 4, 8, 19]), and Curiosity (e.g., ChemCam [17]), have indicated the presence of more felsic rocks. Through the utilization of CRISM, feldspathic rocks have been reported across the surface of Mars from Camichel crater in Xanthe Terra [14], which is located far to the west of the region being examined and discussed here and north of Valles Marineris, and surrounding areas [11, 21], to light-toned, polygonally fractured outcrops exposed within flat-floored impact craters, as well as other exposures (e.g., buttes and crater rims), positioned throughout the Noachian-aged southern highlands [6, 22]. These previously observed occurrences can be classified as either a relatively unaltered feldspathic rock or an altered material consisting of primarily feldspar and (Al, Fe, Mg)-phyllosilicates. Presented here are newly observed occurrences of feldspar-rich material (sites circled in white) that span the entirety of the study region from site 2 to 30 depicted below in Figure 1.

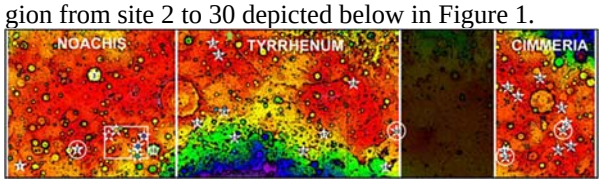

Figure 1. MOLA basemap highlighting previously reported occurrences of feldspar-rich material demarcated by light green circles [22], light blue circles [6], and a dark red star [17] in the portion of the southern highlands bounded above. The white box shows the spatial extent of the study region from [22] and its location within the region being examined here. The sites demarcated by the colored circles correspond to sites 4 (red), 5 (orange), 6 (yellow), 7 (green), 8 (blue), and 9 (purple) in this study. No craters were chosen for analysis in the blacked-out portion of the map.

Data and Methodology: The mineralogical composition of wind-eroded floor materials, as well as exposed stratigraphic layers and other corresponding geological units, contained within and located in close proximity to (i.e., within ~100 km of the crater rim of) thirty Noachian-aged impact craters (demarcated by numbered white stars in Figure 1 and binned into their respective labeled study areas) in the Martian equatorial highlands (between 0–30°S, 0–165°E) were investigated by utilizing the CRISM instrument aboard MRO. These sites were selected through a survey of flat-floored craters in the southern highlands by R. P. Irwin III, who documented all available MRO imaging (e.g., CRISM, CTX, and HiRISE). With respect to CRISM data, the most recent versions of the TRDRs (i.e., TRR3s) were primarily used in lieu of initial MRDR analysis. For which, both FRT (18 m/pixel) and HRL (36 m/pixel) data products were examined to determine the presence and spatial extent of relevant exposures. Geographically, the abovementioned subset of craters lies to the north of Hellas Basin and spans three different regions of the Martian surface, which includes Noachis Terra (20–55°E), Tyrrhena Terra (55–100°E), and Terra Cimmeria (120–140°E), which constitutes some of the least dust-covered areas in the highlands [16]. Particular attention was payed to sites where feldspar-rich material was tentatively detected through the use of the updated CRISM summary products [20], specifically the spectral parameter (i.e., BD1300) formulated to determine the presence of the 1.3 μm absorption feature associated with minor amounts of Fe^{2+} substituting for Ca^{2+} within the framework structure of feldspars [5]. Spectral analyses using CAT for ENVI was then performed to confirm the presence of a feldspar component in abundances greater than 95% [7, 13] for smaller feldspar grains (i.e., sub-500 μm) or 50% [15] for larger grains (i.e., greater than 840 μm in size).

Primary Results and Discussion: Two of the four sites where feldspar-rich rocks were identified are shown below in Figures 2 and 3. As displayed in Figure 1, these sites are in Tyrrhena and Cimmeria respectively and represent both unaltered and altered feldspathic rock. *Mineral Mapping*. Panel A in Figures 2 and 3 show an enhanced true color representation of the scenes, while panel B allows for the visualization of feldspathic material along with other associated mineral phases by employing a custom browse product. The areas encircled in black, and indicated by the colored arrows, in the TRU browse products show the approximate location of the ROIs that produced the spectra plotted in panel C. The exposures observed in a complex crater located to the northwest of site 20 (Kamativi) appear to be relatively small, light-toned outcrops of brecciated rocks in and around the central peak that have been exhumed from a smooth covering material that is spectrally distinct from the blocks themselves. Site 22 corresponds to an infilled, and capped, flat-floored unnamed crater. The exposure of interest associated with this site is a fractured, light-toned outcrop located in the southern portion of the crater, which appears to be overlaid by a spectrally bland dark-toned layer. This outcrop is similar geomorphologically to those reported by [22]. These exposures appear yellow in the CUSTOM browse product shown in panel B Figure 2 and red in Figure 3.

Mineral Identification. The feldspathic outcrops observed at sites 20 and 22 were identified as such based on the presence of the characteristic ~1.25 μm absorption in the NIR, which can vary in position and depth depending on the weight percent of FeO, the $NaAlSi_3O_8$ (albite) to $CaAl_2Si_2O_8$ (anorthite) ratio [1], and the particle size. An increase in iron content and/or particle size can result in the feature shifting to longer wavelengths and an increase in the band depth [18], however a change in composition to a more sodic-rich feldspar can cause the band position to shift to shorter wavelengths and become less apparent [2]. As seen in Figure 2 panel C, the absorption associated with feldspar can also occur with other features that indicate the presence of a related mineral phases or indicative of alteration. Additional absorptions at ~1.42 μm, ~1.91 μm, and ~2.54 μm in the CRISM I/F spectra suggest the presence of the zeolite analcime when compared to a similar spectrum from the most recent USGS spectral library [9]. Unlike the identification of analcime, the feldspar-related feature present in all the spectra shown here can indicate any feldspar phase, from alkali to plagioclase, that contains a minor fraction of Ca-bearing feldspar for which Fe^{2+} has been substituted [10]. This is demonstrated in panel C Figure 3, which compares USGS laboratory spectra for two feldspar endmembers that contain a minute and substantial amount of Fe^{2+}-bearing anorthite, and can be interpreted as the small anorthite fraction of the orthoclase sample contains substituted ferrous iron, thereby accounting for the absorption that occurs near 1.3 μm.

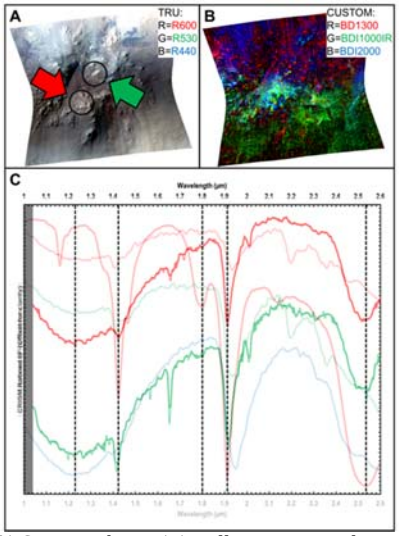

Figure 2. (A) Same as above. (B) Yellow corresponds to altered feldspathic material or zeolites (particularly, the Na-zeolite analcime) co-occurring with feldspar, green to crystalline Fe^{2+} silicates (specifically, olivine and (Fe, Mg)-phyllosilicates), cyan to material composed of olivine and high-Ca pyroxene, and blue to pyroxene (both low- and high-Ca). (C) The partially transparent red, green, and blue spectra with characteristic ~1.25 μm absorption feature corresponds to USGS laboratory spectra for albite, oligoclase, and bytownite with minor Fe^{2+} substitution, while the red spectrum with the prominent ~2.54 μm feature is representative of a typical analcime spectrum.

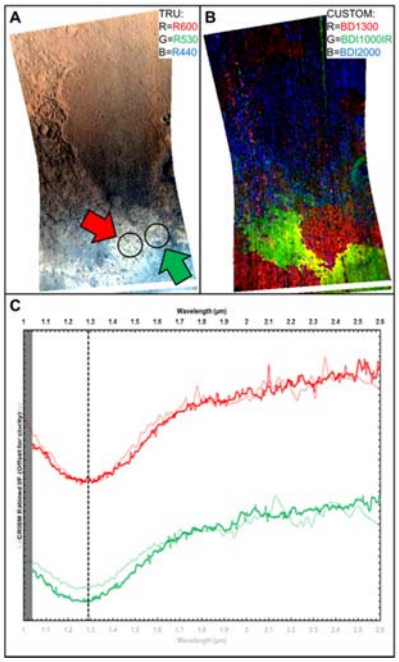

Figure 3. (A) The red and green arrows pointing to the black circled areas within the observation correspond to where the similarly colored spectra shown in panel C were collected. (B) Red corresponds to unaltered feldspathic material, yellow to altered feldspathic material or crystalline Fe^{2+} silicates co-occurring with feldspar, green to crystalline Fe^{2+} silicates (specifically, olivine in this image), and blue to pyroxene (both low- and high-Ca varieties). (C) The partially transparent red and green spectra are comparable USGS library spectra for anorthite (Ca-rich endmember) and Fe-rich orthoclase (K-rich endmember of the alkali feldspar series) respectively.

Conclusion: This study expands upon the previous reported detections of feldspathic material observed on the surface of Mars (both numerically and spatially), as well as adding to recent studies that have reported the presence of other minerals (as alteration products or co-occurring phases) in association with feldspar. Finally, the presence of Fe^{2+}-bearing anorthite within a primarily alkali feldspar sample can result in the ~1.3 μm feature.

References: [1] Adams, J. B. (1975) *Infrared and Raman spectroscopy of lunar and terrestrial minerals*, 91-116. [2] Adams, J. B. and Goullaud, L. H. (1978) *LPS IX*, 2901-2909. [3] Bandfield, J. L. et al. (2004) *JGR: Planets*, *109*, E10009. [4] Bandfield, J. L. (2006) *GRL*, *33*, L06203. [5] Burns, R. G. (2005) *Mineralogical applications of crystal field theory*. [6] Carter, J. and Poulet, F. (2013) *Nat. Geosci.*, *6*, 1008-1012. [7] Cheek, L. C. et al. (2013) *JGR: Planets*, *118*, 1805-1820. [8] Christensen, P. R. et al. (2005) *Nature*, *436*, 504-509. [9] Clark, R. N. et al., 2007, USGS digital spectral library splib06a: U.S. Geological Survey, Digital Data Series 231. [10] Deer, W. A., Howie, R. A., and Zussman, J. (2001) *Rock-Forming Minerals: Framework Silicates – Feldspars*. [11] Ding, N. et al. (2015) *Icarus*, *252*, 255-270. [12] McSween, H. Y., Taylor, G. J., and Wyatt, M. B. (2009) *Science*, 324, 736-739. [13] Ohtake, M. et al. (2009) *Nature*, *461*, 236-240. [14] Popa, C., Esposito, F., and Colangeli, L. (2010) *LPS XLI*, Abstract #1807. [15] Rogers, A. D. and Nekvasil, H. (2015) *GRL*, *42*, 2619-2626. [16] Ruff, S. W. and Christensen, P. R. (2002) *JGR: Planets*, *107*, 5127. [17] Sautter, V. et al. (2015) *Nat. Geosci.*, *8*, 605-609. [18] Serventi, G. et al. (2013) *Icarus*, *226*, 282-298. [19] Smith, M. R. and Bandfield, J. L. (2012) *JGR: Planets*, *117*, E06007. [20] Viviano-Beck, C. E. et al. (2014) *JGR: Planets*, *119*, 1403-1431. [21] Viviano-Beck, C. E. et al. (2017) *Icarus*, *284*, 43-58. [22] Wray, J. J. et al. (2013) *Nat. Geosci.*, *6*, 1013-1017.